

pubs.acs.org/ac Article

Ion Mobility-Mass Spectrometry and Collision-Induced Unfolding Rapidly Characterize the Structural Polydispersity and Stability of an Fc-Fusion Protein

Rosendo C. Villafuerte-Vega, Henry W. Li, Addison E. Bergman, Thomas R. Slaney, Naresh Chennamsetty, Guodong Chen, Li Tao, and Brandon T. Ruotolo*



Cite This: Anal. Chem. 2024, 96, 10003-10012



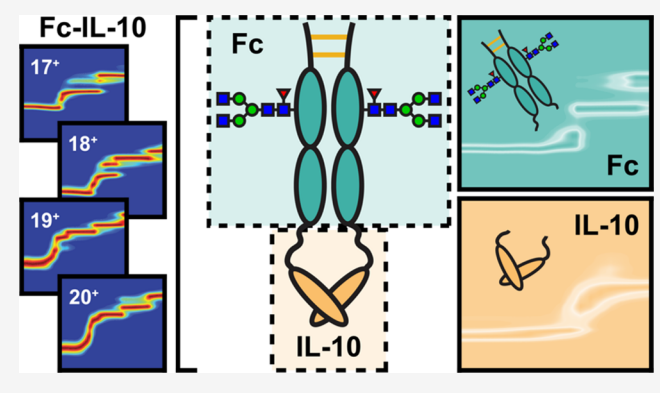
ACCESS

Metrics & More

Article Recommendations

s Supporting Information

ABSTRACT: Fc-fusion proteins are an emerging class of protein therapeutics that combine the properties of biological ligands with the unique properties of the fragment crystallizable (Fc) domain of an immunoglobulin G (IgG). Due to their diverse higher-order structures (HOSs), Fc-fusion proteins remain challenging characterization targets within biopharmaceutical pipelines. While high-resolution biophysical tools are available for HOS characterization, they frequently demand extended time frames and substantial quantities of purified samples, rendering them impractical for swiftly screening candidate molecules. Herein, we describe the development of ion mobility-mass spectrometry (IM-MS) and collision-induced unfolding (CIU) workflows that aim to fill this technology gap, where we focus on probing the HOS of a model



Fc-Interleukin-10 (Fc-IL-10) fusion protein engineered using flexible glycine-serine linkers. We evaluate the ability of these techniques to probe the flexibility of Fc-IL-10 in the absence of bulk solvent relative to other proteins of similar size, as well as localize structural changes of low charge state Fc-IL-10 ions to specific Fc and IL-10 unfolding events during CIU. We subsequently apply these tools to probe the local effects of glycine-serine linkers on the HOS and stability of IL-10 homodimer, which is the biologically active form of IL-10. Our data reveals that Fc-IL-10 produces significantly more structural transitions during CIU and broader IM profiles when compared to a wide range of model proteins, indicative of its exceptional structural dynamism. Furthermore, we use a combination of enzymatic approaches to annotate these intricate CIU data and localize specific transitions to the unfolding of domains within Fc-IL-10. Finally, we detect a strong positive, quadratic relationship between average linker mass and fusion protein stability, suggesting a cooperative influence between glycine-serine linkers and overall fusion protein stability. This is the first reported study on the use of IM-MS and CIU to characterize HOS of Fc-fusion proteins, illustrating the practical applicability of this approach.

INTRODUCTION

Fc-fusion proteins constitute an emerging class of protein therapeutics that have demonstrated great efficacy across a broad range of pathologies due to their diverse compositions and mechanisms of action. 1-3 Such therapeutic modalities combine the pharmacological properties of a broad range of biomolecules with the distinctive biological functions of the fragment crystallizable (Fc) region of an immunoglobulin G (IgG).^{4,5} The active components of Fc-fusion proteins can be peptides,^{6,7} cytokine traps,³ recombinant enzymes,^{8,9} or the extracellular domains (ECDs) of receptors, 10,11 where most are attached to both chains of the disulfide-linked, dimeric Fc domain. Most notably, Fc-fusion proteins possess increased serum half-life owing to their reduced renal clearance and neonatal Fc-receptor (FcRn)-mediated recycling from endosomes. 12,13 Apart from half-life extension, the Fc domain can also greatly improve the solubility and stability of hydrophobic

biomolecules, increase expression and secretion rates during production, enable facile purification via affinity for Protein A, and elicit Fc-mediated effector functions. 14,15 Combined, these advantages have led to the approval of 13 Fc-fusion proteins by the FDA to date, and approximately 40 therapeutics are currently in clinical development. 16,17

The successful engineering of recombinant Fc-fusion proteins generally necessitates a suitable protein linker since the direct fusion of the Fc with protein domains can

Received: March 15, 2024 Revised: May 2, 2024 Accepted: May 31, 2024 Published: June 10, 2024





compromise appropriate folding and bioactivity. 16 Flexible linkers, which typically consist of glycine (Gly) and serine (Ser) repeats, are most widely utilized due to their tunable length and composition. An increase in Gly residues has been correlated with a decrease in linker rigidity, while an increase in polar residues like Ser has been shown to improve the stability of the linker in aqueous environments by promoting hydrogen bonds with surrounding water. 17,18 This increase in hydrophilicity prevents the formation of secondary structure and minimizes the likelihood of the linker disrupting the proper folding and function of the fusion protein. Within this context, a (Gly4Ser)_n linker is most commonly used, where n can be adjusted to alter the structural flexibility of Fc-fusion proteins and the spatial mobility of protein domains. Thus, the optimal separation of adjacent domains can be achieved, or important interdomain noncovalent interactions can be preserved. 19,20

Indeed, controlling the ultimate structural flexibility of Fcfusion proteins through alterations to their amino acid sequence represents a critical objective in their design and development as therapeutics. Furthermore, the higher-order structures (HOSs) of Fc-fusion protein constructs can be significantly influenced by post-translational modifications (PTMs) and chemical modifications produced under stress conditions, further complicating fusion protein engineering efforts. These alterations in HOS can significantly influence aggregation propensity, immunogenicity, serum half-life, and molecular binding.²¹⁻²⁴ Thus, discovering optimal Fc-fusion protein designs necessitates analytical methodologies capable of quantifying the structural contributions of individual protein domains to overall protein HOS and measuring the local effects of linker length and composition on Fc-fusion protein stability and conformational dynamics. Within this context, conventional high-resolution technologies for protein HOS characterization often require long time scales and complex sample preparation requirements that are not conducive for the rapid screening of candidate molecules, and they often fail to fully capture the diverse conformational ensembles adopted by highly dynamic Fc-fusion proteins.

Over the past two decades, mass spectrometry (MS)-based approaches have emerged as powerful orthogonal tools for the characterization of protein therapeutic HOS and stability in the gas phase. 25,26 For example, ion mobility combined with native mass spectrometry (IM-MS) has been shown to be a valuable technology for the structural analyses of proteins and protein complexes, providing information regarding topologies, stoichiometries, sizes, and shapes, with the latter two properties evaluated primarily through the measurement of rotationally averaged collision cross sections (Ωs).^{27,28} Briefly, IM separates gas-phase protein ions based on their charge and Ω on the millisecond time scale, allowing for the separation of two conformationally different ions that share the same massto-charge (m/z) ratio. Furthermore, collision-induced unfolding (CIU) has enabled IM-MS to simultaneously probe the HOSs and stabilities of iso-cross-sectional proteins by collisionally activating ions to induce unique gas-phase unfolding profiles prior to IM separation.²⁹ Ongoing efforts in the development of native IM-MS and CIU-based workflows for the characterization of protein therapeutics have been successful in classifying IgG subclasses using both intact monoclonal antibodies (mAbs) and large fragments, 30,31 detecting subtle differences between innovator and biosimilar therapeutics,^{32–34} probing the complex structures of engineered multispecific mAbs,^{35,36} and assessing stability shifts

associated with conjugating small molecules to mAb sequences.^{37,38} However, the utility of native IM-MS and CIU in probing the highly dynamic structures of Fc-fusion proteins with flexible linkers remains largely unexplored.

Herein, we describe the first series of gas-phase measurements that leverage IM-MS and CIU to investigate the structural dynamics and stabilities of Fc-fusion proteins engineered with flexible linkers. Specifically, we characterize the HOS and stability of a model Fc-interleukin-10 (Fc-IL-10) fusion protein that links the C-termini of an IgG1 Fc domain with the N-termini of individual monomer units of human IL-10, which biologically exists as homodimer, via a flexible Gly-Ser linker (Figure S1). We observe broadened IM peak widths for Fc-IL-10 ions and compare these data to a series of protein standards ranging from 36 to 150 kDa to quantify the elevated conformational polydispersity of Fc-IL-10. In addition, our CIU data recorded for Fc-IL-10 reveal up to five gas-phase unfolding events, a value that is larger than what is typically observed for larger native protein ions, providing further evidence of the intricate structural ensemble adopted by Fc-IL-10 when compared to model proteins. Our findings allow us to isolate and evaluate HOS contributions from the Fc, IL-10, and Gly-Ser linker units to the overall gas-phase stability of the intact fusion protein. Here, we determined gas-phase stability by quantifying the relative collisional energy required to induce protein unfolding. Specifically, we find that the Fc region of the protein is sustainability more stable than the IL-10 dimer, a result that is strongly correlated with other biophysical measurements. In addition, we use a combination of enzymatic steps to facilitate the modification or complete removal of Fclocalized N-linked glycans. These experiments produced fusion proteins of decreased stabilities, as expected, but stability shifts were observed to unequally influence the CIU transitions, which allowed us to annotate those features most associated with the Fc portion of the model fusion proteins studied here. Finally, we discern a positive, quadratic relationship between average linker length and IL-10 homodimer stability. We conclude our report by discussing the analytical implications of IM-MS and CIU methodologies for delineating the multifaceted biophysical underpinnings of Fc-fusion protein function and advancing future discovery and development efforts within the biopharmaceutical pipeline.

EXPERIMENTAL SECTION

Materials and Sample Preparation. A model Fc-IL-10 fusion protein and a selection of proteins were prepared as described in the Supporting Information.

High-Resolution Native MS. Prepared intact and digested Fc-IL-10 samples (3 to 5 μ L) were directly infused into a standard commercial Q Exactive Orbitrap MS with Ultra High Mass Range (QE-UHMR) platform (Thermo Fisher Scientific, San Jose, CA) via nanoelectrospray ionization (nESI) in positive ion mode using gold-coated borosilicate capillaries $(5-10 \mu \text{m} \text{ i.d., Harvard Apparatus, Holliston, MA})$ prepared in-house with a Sutter P-97 Micropipette Puller (Sutter Instrument, Novato, CA) and Quorum SC7620 mini Sputter Coater (Quorum Technologies, Lewes, U.K.). Source settings were as follows: capillary voltage, 1.2 to 1.4 kV; source temperature, 250 °C; S-lens RF level, 45 to 80. Nitrogen was used as the collision gas, and the trapping pressure was set between 2 and 4. Low m/z detector optimization and high m/ztransfer optics were used. In-source trapping was enabled with desolvation voltages ranging from -20 and -100 V. Additional

removal of nonspecific salt adducts was achieved with the application of in-source collision-induced dissociation (CID) that ranged from 0 to 25 V. For higher-energy collisional dissociation (HCD) of IL-10 homodimer, charge state 13⁺ was first isolated in the quadrupole with an isolation window of 50 m/z. Dissociation of IL-10 homodimer into monomer was then achieved by applying 60 V of collision energy (CE). For partially reduced Fc samples, charge state 17⁺ was isolated in the quadrupole with an isolation window of 50 m/z and then dissociated into Fc/2 fragments with 100 V of CE. All QE-UHMR spectra were collected with a noise threshold of 4.64, a resolution of 12,500 at m/z 400, an AGC target of 2 × 10⁵, and a maximum injection time of 200 ms. Five microscans were combined into a single scan, and between 50 and 100 scans were averaged for each spectrum. All data were then processed and deconvoluted using UniDec.³⁹ The NIST Mass and Fragment Calculator was utilized to calculate theoretical masses using International Union of Pure and Applied Chemistry (IUPAC) average elemental atomic masses.

Native IM-MS and CIU. Synapt G2 HDMS. Piloting IM-MS and CIU experiments were performed on a quadrupole-ion mobility-time-of-flight mass spectrometer (Q-IM-ToF-MS) (Synapt G2 HDMS, Waters, Milford, MA). Samples (3 to 5 μ L) were loaded into in-house gold-coated borosilicate capillaries, and ions were generated by direct infusion using a nESI source in positive ion mode. Settings throughout the instrument were optimized to improve the desolvation and transmission of native-like protein ions prior to IM separation: capillary voltage, 1.2 to 1.4 kV; source temperature, 25 °C; sample cone, 20 to 40 V; extraction cone, 0 V; trap collision voltage (CV), 5 V; and trap DC bias, 35 to 45 V. The capillary tip was positioned 5-10 mm from the cone orifice for all MS experiments, depending on the capillary voltage used. 41 Backing pressure was set to ~7 mbar for improved ion transmission for all samples. Gas flows (mL/min) were as follows: source, 50; trap, 10; helium cell, 200; and travelingwave ion mobility (TWIM) separator, 90. The trap travelingwave ion guide was pressurized to 4.96×10^{-2} mbar of argon gas, and the TWIM separator was pressured to ~3.43 mbar of nitrogen gas. TWIM separation was achieved with a travelingwave height and velocity of 40 V and 600 m/s, respectively. The ToF-MS was operated in the 1000 to 12,000 m/z range in sensitivity mode at a pressure of 2.4×10^{-6} mbar. CIU experiments were performed for intact Fc-IL-10 and NISTmAb samples by subjecting ions to collisions in the traveling-wave ion trap prior to IM separation. Here, CVs were ramped from 5 to 200 V in 5 V intervals. PolyA, BSA, and ADH ions were used as $^{\text{TW}}\Omega_{\text{N}2}$ calibrants. 42

SELECT SERIES Cyclic IMS. IM-MS and CIU experiments for the GlySERIAS digests of Fc-IL-10 were performed on a quadrupole-cyclic ion mobility-time-of-flight mass spectrometer (Q-cIM-ToF-MS) (SELECT SERIES Cyclic IMS, Waters, Milford, MA) to better resolve linker length populations that remained attached to IL-10 and Fc domains. Details of this instrumentation and its operation have been described previously. Samples (3 to 5 μ L) were loaded into inhouse gold-coated borosilicate capillaries, and ions were generated via nESI in positive ion mode. The quadrupole profile was set to manual and tuned to improve the transmission of IL-10 homodimer and Fc ions. As in our Synapt G2 experiments, cIM-MS settings were optimized to transmit ions without excessive activation prior to cIM separation: capillary voltage, 1.2 to 1.3 kV; source temperature,

25 °C; sample cone, 0 V; source offset, 0 V; trap CV, 5 V; and post-trap bias, 35 V. These soft ionization parameters were essential to prevent significant activation of IL-10 homodimer. Gas flows (mL/min) were as follows: ion guide, 35; trap, 7; helium cell, 150; and cIM separator, 45. The backing pressure was 2.53 mbar. The trap traveling-wave ion guide was pressured to 3.95×10^{-2} mbar of nitrogen gas. The cIM separator was pressured to ~1.76 mbar of nitrogen gas, and cIM separation was achieved using a single pass with a wave height and velocity of 30 V and 375 m/s, respectively. A full list of settings for the multifunction array region is given in Table S1. The ToF-MS was operated in the 50 to 8,000 m/zrange in V-mode at a pressure of 4.9×10^{-7} mbar. CIU experiments were performed by ramping the CVs in the trap region from 4 to 160 V in 4 V intervals prior to cIM separation. PolyA and BSA ions were used as ${}^{TW}\Omega_{N2}$ calibrants. 42

Data Processing and Analysis. IM and MS spectra were viewed using Driftscope v3.0 and Masslynx v4.2 software, respectively (Waters, Milford, MA). Mass spectra were deconvoluted using UniDec.³⁹ Arrival time distributions (ATDs) were extracted and converted to ${}^{\text{TW}}\Omega_{\text{N2}}$ using a modified version of CIUSuite 2 (v2.3),45 which encodes both TWIMExtract⁴⁶ and IMSCal⁴² for semiautomated drift time extractions and $^{\text{TW}}\Omega_{\text{N2}}$ calibrations, respectively. When comparing the relative stabilities of Fc and IL-10 homodimer subunits generated using GlySERIAS, we need to account for the higher-energy collisions experienced by higher charge states. Therefore, we converted the CV axes of applicable CIU files to laboratory frame energies (E_{lab}) as previously described.⁴⁷ All data were then further processed using the modified CIUSuite 2 software discussed above. CIU fingerprints were subjected to 2-D smoothing using a Savitzky-Golay function with a smoothing window of 5 and 2 smoothing iterations. The CV axis was interpolated with a scaling factor of 4 for Fc CIU data, while no interpolation was performed for intact Fc-IL-10 and IL-10 homodimer CIU data. Standard feature detection was performed using a minimum feature length of 2 steps and an allowed width of 1 to 1.5 nm² in $^{\text{TW}}\Omega_{\text{N2}}$ axis units. CIU₅₀ values were then computed using max centroiding mode with a transition padding of 15 V and a maximum CV gap length of 0. Root-mean-square-deviation (RMSD) analysis was performed using the compare function within CIUSuite 2, and RMSD factor differences, where applicable, were calculated as previously described.⁴⁸ All CIU fingerprints shown are the average of three technical replicates with baseline RMSDs of <5%. We define a technical replicate as a repeated measurement using the same sample and/or capillary taken on the same day of an experiment. $^{\mathrm{TW}}\Omega_{\mathrm{N2}}$ distributions of IM-MS data, where applicable, were fitted with a Gaussian function using Fityk curve fitting software. 49 Data visualization and statistical analyses of IM-MS and CIU quantitative data were performed using GraphPad Prism (San Diego, CA). For statistical analyses, we specifically used a one-way ordinary analysis of variance (ANOVA) with Tukey correction for multiple comparisons to analyze differences between three or more experimental data sets using an α value of 0.05. When comparing only two data sets, we performed a simple t test using an α value of 0.05. All error bars correspond to the standard deviation of three technical replicates unless otherwise stated.

RESULTS AND DISCUSSION

Native IM-MS and CIU Probe the Structural Dynamics of Fc-IL-10 in the Gas Phase. IL-10 is a potent immunoregulatory cytokine that plays a critical role in modulating inflammatory responses and preserving cell homeostasis. 50,51 Structurally, its biologically active form is a domain-swapped, noncovalent 37 kDa homodimer made of two intertwining monomers, each consisting of six α -helices (A-F) stabilized by two intrachain disulfide bonds. 52,53 The domain-swapped dimeric nature of IL-10, which involves helices E and F from one monomer penetrating into the hydrophobic cleft of helices A-D of the other monomer, is pivotal for proper receptor binding.⁵⁴ However, IL-10 homodimer is known to be unstable owing to its short halflife and facile degradation in vivo, limiting its clinical applications. 55,56 The Fc-IL-10 fusion protein in this work addresses this limitation by extending the half-life of IL-10 through FcRn-mediated recycling from endosomes. Importantly, the use of a flexible Gly-Ser linker permits the spatial mobility of IL-10 monomeric units, increasing their likelihood to interact and form the biologically active homodimer (Figure S1). Within this scope, characterizing the HOS of Fc-IL-10 with current measurement technologies remains a major challenge, as its unique engineering complicates its structure and dynamics.

Although there is no full-length Fc-IL-10 structure derived from X-ray crystallography, NMR, or Cryo-EM, we successfully leverage IM-MS and CIU to rapidly extract structural information on Fc-IL-10 by monitoring its conformational ensemble and stability in the gas-phase. We first generated Fc-IL-10 ions via nESI under conditions that typically preserve compact, native-like ions that closely resemble the structural states in solution.^{28,41} Under these conditions, Fc-IL-10 adopted a narrow charge state distribution (16+ to 22+) allowing us to measure an intact molecular weight (M_W) of ~94 kDa (Figure 1A). We also observed noncovalent dimeric Fc-IL-10 aggregates that are likely representative of those found in solution. 57,58 Our measurements indicate that these dimers are present in low abundance (1.79 \pm 0.08% of total monomer and dimer signal), and are likely dependent upon the solution conditions used to prepare our Fc-IL-10 samples prior to native IM-MS measurements.⁵⁹

To benchmark our native IM-MS measurements of Fc-IL-10, we compared its ${}^{TW}\Omega_{N2}$ values to those obtained for a series of native protein standards ranging from 36 to 150 kDa in molecular mass (Figure 1B). The average relative standard error (RSD) for technical replicates of these measurements was $0.06 \pm 0.05\%$, and comparisons to reported $^{\text{TW}}\Omega_{\text{N2}}$ literature values (excluding NISTmAb fragments) yielded an average difference of $-0.28 \pm 1.68\%$ (abs. Avg diff. of $1.28 \pm 1.13\%$) (Figure S2 and Table S2). For Fc-IL-10, we observed an average $^{TW}\Omega_{N2}$ of 55.2 \pm 2.0 nm² across all charge states, which is similar to the ${}^{TW}\Omega_{N2}$ values obtained for proteins of similar $M_{\rm W}$ (F(ab')₂, ~98 kDa; ConA tetramer, ~103 kDa) as observed previously. However, when we considered the IM resolving power (R_p) of our $^{\text{TW}}\Omega_{N2}$ distributions, we noticed drastic differences between Fc-IL-10 and other proteins (Figure 1C). Here, we define R_{p} as the centroid ${}^{T\hat{W}}\Omega_{N2}$ of our IM distributions divided by their full width at halfmaximum (fwhm), $R_p = \Omega/\Delta\Omega$. We found that the average R_p for the three most abundant charge states of Fc-IL-10 (19⁺ to 21⁺) was approximately 50 and 66% less than that of F(ab')₂

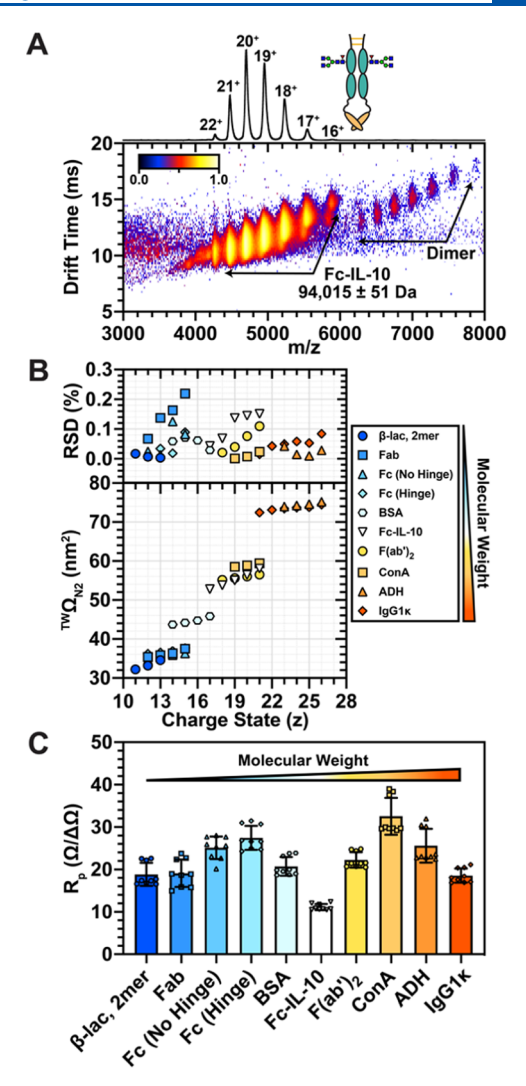


Figure 1. Native IM-MS measurements of Fc-IL-10 and a series of protein standards on a Waters Synapt G2 HDMS IM-MS platform. (A) Representative IM-MS spectrum of Fc-IL-10 reveals a narrow charge state distribution ranging from 16⁺ to 22⁺. (B). $^{\text{TW}}\Omega_{\text{N2}}$ values for native Fc-IL-10 and protein standards as a function of charge state. Corresponding RSDs (<0.3%) are shown for technical replicates (n = 3). (C) R_{p} ($\Omega/\Delta\Omega$) of Fc-IL-10 and protein standards. IM R_{p} values extracted from the three most prominent charge states observed for each protein in triplicate (n = 9).

and ConA tetramer, respectively. These differences, which result from the wider ${}^{TW}\Omega_{N2}$ distributions of Fc-IL-10 (Figure S3), suggest that Fc-IL-10 is likely trapped in a wider array of solution conformations during nESI than the equivalently sized proteins measured in our survey. Interestingly, the R_p of Fc-IL-10 is also lower than that of NISTmAb ($IgG1\kappa$), differing by approximately 40%. Previous studies have shown that mAbs are inherently more flexible and dynamic than comparably sized protein complexes in terms of $M_{
m W}^{~60,61}$ Our results are consistent with these previously reported observations, as NISTmAb adopts a wider range of conformations than ADH, which is similar in $M_{\rm W}$ (~148 kDa) and $^{\rm TW}\Omega_{\rm N2}$. We propose that the Gly-Ser linker, combined with the HOSs of individual Fc and IL-10 domains, significantly contribute to the overall flexibility of Fc-IL-10 compared to NISTmAb, as evidenced by its lower IM R_p and wider ${}^{TW}\Omega_{N2}$ distributions.

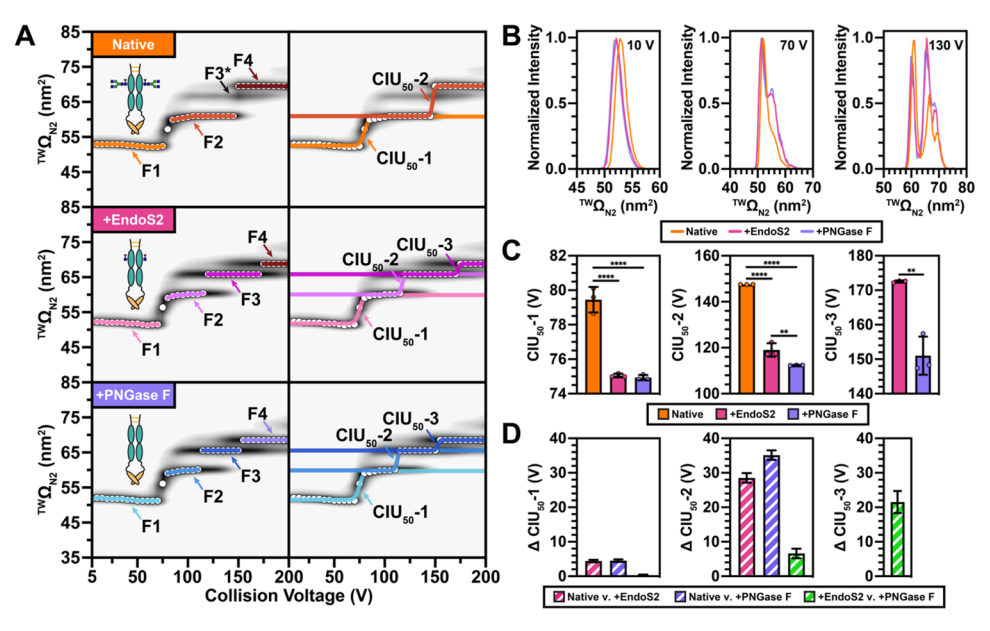


Figure 2. CIU experiments of Fc-IL-10 before and after treatment with EndoS2 or PNGase F. (A) CIU fingerprints for charge state 17^+ . Features are detected by CIUSuite 2 (v2.3) (left) and subsequently utilized for CIU $_{50}$ stability quantitation (right). Feature three (F3*) in native Fc-IL-10 is labeled but omitted during the fitting of CIU $_{50}$ data. (B) $^{\text{TW}}\Omega_{\text{N2}}$ distributions of native and deglycosylated Fc-IL-10 at different trap collision voltages. More extended conformations increase in intensity with sequential removal of sugar moieties. (C) CIU $_{50}$ analyses (n=3) of each transition reveal significant destabilization of Fc-IL-10 after deglycosylation (**p < 0.01, **** < 0.0001). (D) Plots of mean differences in CIU $_{50}$ values. Error bars of these mean differences are given in SEM obtained using a one-way ordinary ANOVA with Tukey correction for multiple comparisons within GraphPad Prism.

To further probe the conformational dynamics of Fc-IL-10, we performed CIU on charge states 17⁺ to 21⁺ (Figure S4). Compared to previously reported CIU data acquired for ConA tetramer 62,63 and F(ab')₂ fragment ions, 64,65 which collectively only adopt up to four features during CIU, our CIU data for Fc-IL-10 qualitatively reveal three to six prominent features, further indicating the increased level of dynamism in Fc-IL-10 when compared to model proteins of similar M_W . The ultimate number of CIU transitions we observe in Fc-IL-10 is also higher than that of NISTmAb (Figure S5), further underscoring the relatively diverse structural ensemble adopted by Fc-IL-10. Previous studies have established a strong, positive correlation between the number of domains within a protein structure and the number of CIU transitions observed. 66,67 Given this correlation, it is likely that Fc-IL-10 supersedes such a trend and produces subdomain correlated unfolding in many of our CIU data sets.

Enzymatic Approaches Assist in the Annotation of Fc-IL-10 CIU Pathways. To establish a mechanistic understanding of Fc-IL-10 CIU, we designed a series of experiments aimed at evaluating its domain-level stabilities and assigning protein domains or regions to specific CIU transitions. First, we enzymatically removed the N-glycans attached within the C_H, regions of the Fc domain of Fc-IL-10, as these regions have been shown to become destabilized after N-glycan removal.⁶⁸⁻⁷¹ Deglycosylation was achieved using either EndoS2, which leaves the core *N*-acetylglucosamine (GlcNAc) intact, or PNGase F, which completely hydrolyzes all Nglycans and deamidates the asparagine residue to produce aspartic acid. To monitor the progress of our deglycosylation reactions, we performed native orbitrap MS measurements to resolve individual glycoforms of Fc-IL-10 before and after the addition of each respective endoglycosidase (Figure S6 and Table S3). Our results for fully glycosylated Fc-IL-10

demonstrate the presence of various expected glycoforms (G0F, G1F, and G2F) that are commonly located in the Fc portion of therapeutic antibodies, as well as a small amount of afucosylated sugar structures (Figure S6A).⁷² Upon EndoS2 treatment, we successfully achieved the hydrolysis of the glycan structures after the core GlcNAc with or without the core fucose (Fuc) (Figure S6B). Incubation with PNGase F, on the other hand, efficiently removed all *N*-glycans (Figure S6C).

We proceeded with CIU experiments of Fc-IL-10 before and after endoglycosidase treatment. In general, we observe that lower charge states generate CIU transitions that strongly correlate with domain-specific unfolding. 66,67 In contrast, higher charge states experience increased Coulombic strain in the gas phase, leading to more unfolding transitions upon collisional heating.⁷³ As such, we chose to focus on charge state 17⁺ due to its relatively compact low-energy structure, more pronounced extended conformations, and easily quantifiable CIU₅₀ transitions (Figure 2A). CIU fingerprints for native and deglycosylated Fc-IL-10 show the presence of three or four prominent conformational intermediates corresponding to two or three unfolding events, respectively. We detect a minor CIU feature with a $^{\text{TW}}\Omega_{\text{N2}}$ of \sim 66.5 nm² for the native, fully glycosylated Fc-IL-10. However, given the relatively low intensity of this feature, we have focused on the more intense feature with a $^{TW}\Omega_{N2}$ of ~69.5 nm² (feature four). We notice the greatest differences in the $^{TW}\Omega_{N2}$ distributions of native and deglycosylated Fc-IL-10 at higher trap collision voltages, where more extended conformations increase in intensity upon glycan removal (Figure 2B). We also observe prominent shifts in CIU₅₀-2 and CIU₅₀-3 values upon deglycosylation, suggesting a connection between these stability values and the Fc region of the fusion protein. This trend was general across the other Fc-IL-10 charge states detected (Figure S7). A quantitative analysis of CIU₅₀ values further supports these qualitative observations of 17⁺ ions, where CIU₅₀-1 values of

EndoS2 (75.05 \pm 0.10 V) and PNGase F (74.93 \pm 0.16 V) treated samples were less than those of native Fc-IL-10 (79.45 \pm 0.74 V) (Figure 2C). When we compare the CIU₅₀-1 stabilities between EndoS2 and PNGase F treated samples, however, we see no statistically significant changes in the CIU₅₀-1 values recorded, indicating that the PNGase F-driven removal of core GlcNAc and Fuc residues, which are conserved with EndoS2, do not induce stability shifts associated with this CIU transition. Conversely, removal of these core sugars greatly destabilizes the structures adopted by Fc-IL-10 at higher collision energies. We measure significant shifts in CIU₅₀-2 values that decrease with the successive removal of Nglycans (Native, 147.50 \pm 0.01 V; EndoS2, 119.00 \pm 2.93 V; PNGase F, 112.40 \pm 0.10 V). The features that define CIU₅₀-3 exclusively appear in deglycosylated samples, where comparable decreases in stability are observed after the removal of core GlcNAc and Fuc sugars using PNGase F. By plotting the mean differences in CIU50 values recorded across all transitions observed in our data set (Figure 2D), we are able to achieve a clearer annotation of our Fc-IL-10 CIU data. In brief, we quantify the greatest shifts in CIU₅₀ values at higher-energy transitions, where CIU_{50} -2 and CIU_{50} -3 values shift by ~35 and ~21% after complete N-glycan removal, respectively. CIU_{50} -1 values, on the other hand, only shift by ~5%. Taken together, these results permit us to confidently assign CIU₅₀-2 and CIU₅₀-3 transitions for Fc-IL-10 as related to the unfolding of the Fc.

We continued our efforts to annotate Fc-IL-10 CIU transitions by enzymatically digesting the fusion protein into Fc and IL-10 fragments using GlySERIAS, a unique enzyme that specifically cleaves flexible linkers rich in Gly and Ser residues. Analysis of these digests by native orbitrap MS showed that the enzymatic reaction liberates the IL-10 homodimer from the Fc (Figure 3). The Gly-Ser linker in

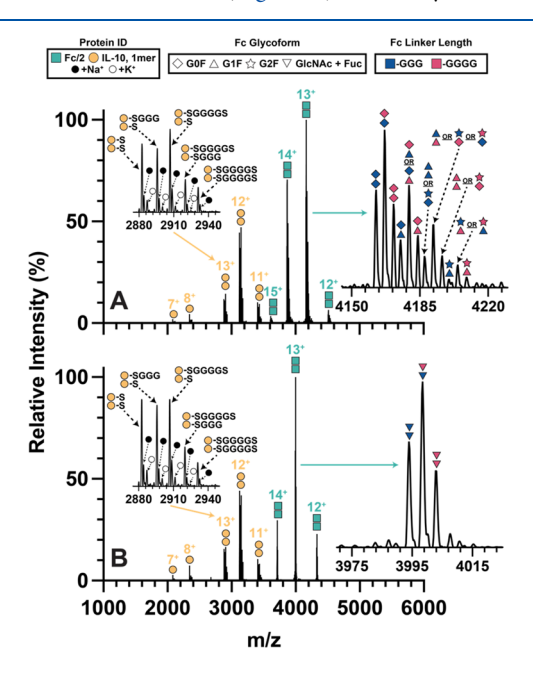


Figure 3. Representative MS spectra of Fc-IL-10 digested with GlySERIAS with or without EndoS2. Zoomed-in spectra of nonreduced Fc subunits show different glycoforms and linker variants (A) before and (B) after treatment with EndoS2. Zoomed-in spectra of IL-10 homodimer show comparable linker variants across both sample prep conditions.

this work contains many potential cleavage sites for GlySERIAS, which generated several variants of Fc and IL-10 with different numbers of Gly and Ser residues attached. Specifically, we observed IL-10 homodimers in five main variant forms, where each monomer possessed one of three main linker tails: S, SG₃, or SG₄S. These assignments were confirmed by dissociating IL-10 homodimer ions to monomers using HCD, where we are able to confidently detect each monomeric variant with S, SG₃, or SG₄S linker tails (Figure S8). The native MS data collected reveals primarily homodimer signals, as expected for IL-10.⁵² We also observed linker polydispersity following GlySERIAS treatment within the Fc subunit, but the presence of different glycoforms complicated GS linker identification (Figure 3A). To reduce sample complexity, Fc glycans were removed using EndoS2, permitting us to detect two main linker tails: G₃ and G₄ (Figure 3B). These findings assisted us in assigning our mass spectra for fully glycosylated Fc, where we identified similar linker variants to those observed after EndoS2 treatment. To confirm our assignment of GS linker variants attached to the Fc subunit, we subjected partially reduced Fc, where only hinge disulfide bonds were reduced, to HCD (Figure S9). Upon dissociation, we were successfully able to detect Fc/2 ions attached to both G₃ and G₄ linker tails, which matched our native MS results for nonreduced Fc fragments. Deconvoluted masses of all species detected during these experiments are summarized in Table S4. We attribute the differences between theoretical and experimental masses observed to insufficient removal of PBS buffer salts used for GlySERIAS digestion, as both sodium and potassium adducts are evident in our native MS spectra.

Next, we leveraged the higher ToF-MS resolution of the SELECT SERIES Q-cIM-ToF-MS platform to better resolve the Fc and IL-10 linker variants detected in our orbitrap native MS data. Despite lower baseline resolution, cIM-MS analysis generates comparable MS spectra, where we are able to delineate all linker variants for both Fc and IL-10 subunits (Figures 4A and S10). Collectively, the $^{TW}\Omega_{N2}$ distributions of IL-10 homodimer revealed at least two conformational families, while cIM-MS detects only one IM feature for Fc, including for samples subjected to deglycosylation with EndoS2 (Figure S11). These differences in ${}^{TW}\Omega_{N2}$ distributions underscore that the IL-10 homodimer exhibits a conformational ensemble of greater polydispersity when compared to the Fc. These results, in part, suggest that the conformational ensemble of the IL-10 homodimer strongly contributes to the structural polydispersity of native, intact Fc-IL-10. Interestingly, the relative intensity of the most extended conformer for IL-10 homodimer increases as we approach higher charge states. This trend is likely the result of the higher local Coulombic strain experienced by the protein ions occupying higher charge states, leading to partial unfolding even under gentle conditions. However, the interdomain connection between helices D and E of IL-10 has been shown to be potentially flexible.⁵² Therefore, the existence of two conformers of IL-10 homodimer in our IM data could be the direct result of this inherent flexibility. The flexibility of IL-10 homodimer is further reflected in our CIU data, where IL-10 ions readily unfold at considerably lower E_{lab} values (<700 eV) when compared with Fc subunit ions (Figure 4B-D). Interestingly, we observe a bimodal distribution of unfolded intermediates for IL-10 homodimer ions just below 650 eV. We suspect that the IL-10 homodimer precursors shown in

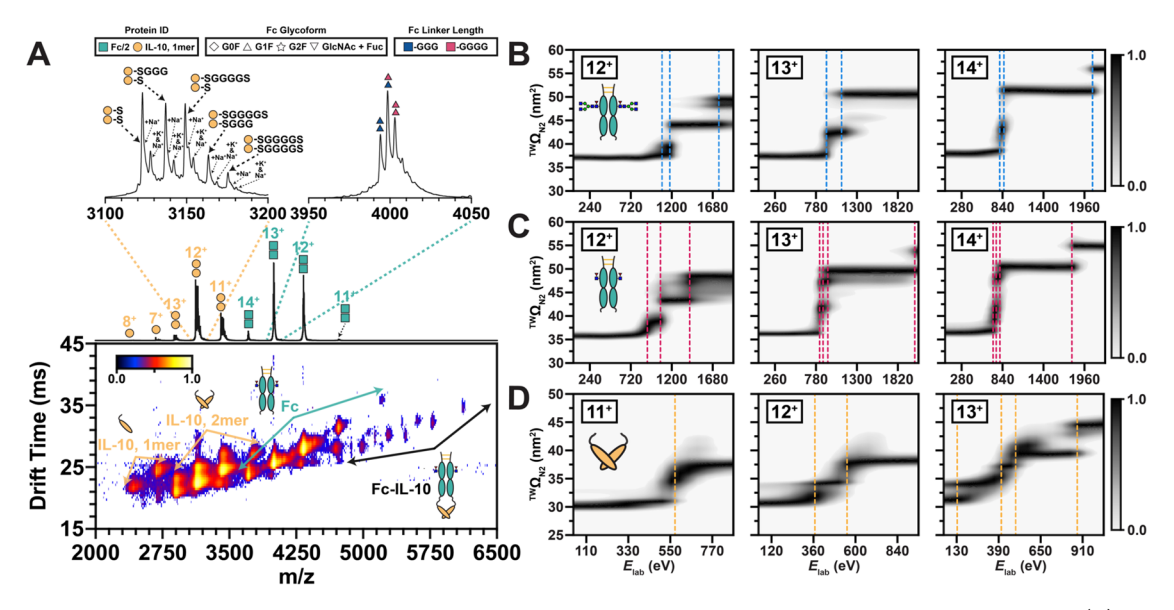


Figure 4. IM-MS and CIU measurements of Fc-IL-10 GlySERIAS digests on a Waters SELECT SERIES cIM-MS platform. (A) Representative cIM-MS spectrum of Fc-IL-10 digested with GlySERIAS and EndoS2 at 5 V of trap CE. Zoomed-in spectra show the linker and glycoform polydispersity present in nonreduced Fc and IL-10 homodimer subunits. CIU fingerprints of (B) native Fc, (C) deglycosylated Fc, and (D) IL-10 homodimer subunits. Dashed blue, red, and yellow lines correspond to CIU transitions for native Fc, deglycosylated Fc, and IL-10 homodimer, respectively.

Figure S11 undergo unique CIU pathways that lead to different unfolded intermediates that vary across charge states, and a portion of these intermediates readily dissociate into IL-10 monomer. Regarding Fc subunits, we observe shifts in gasphase stability after glycan removal with EndoS2 across all CIU₅₀ transitions as expected. Despite these shifts in stability, a quantitative analysis of the first transition (CIU₅₀-1) reveals that IL-10 homodimer initially unfolds at significantly lower $E_{\rm lab}$ values (Av. 372.52 \pm 168.25 eV) than Fc domains (Native, Av. 942.56 \pm 156.03; EndoS2 treated, Av. 815.99 \pm 82.05 eV) when accounting for data acquired across all charge states (Figure S12). Collectively, these results indicate that lower-energy CIU transitions observed in intact Fc-IL-10 ions are most likely related to unfolding within the IL-10 homodimer upon collisional heating.

Flexible Linkers of Different Lengths Induce Subtle Changes in IL-10 Homodimer CIU. Flexible Gly-Ser linkers have been shown to improve the folding and stability of fusion proteins. ¹⁹ To probe local changes in Fc-IL-10 subunit stability as a function of linker length, we extracted the ${}^{\mathrm{TW}}\Omega_{\mathrm{N2}}$ distributions generated during CIU for each Fc and IL-10 homodimer linker variant observed in our cIM-MS spectra by utilizing a narrower m/z extraction window within TWIMExtract. Using the cIM-MS platform was crucial for this analysis, as linker variants could not be sufficiently resolved on our linear TWIM platform. Here, we only conducted our analysis targeting Fc subunits that had been deglycosylated with EndoS2, as native Fc subunits yielded poorly resolved linker variant populations on our cIM-MS platform. Importantly, we saw no changes in Fc subunit stability as the length of the linker tail increased. In contrast, we noticed significant differences in global IL-10 homodimer HOS and stability as the length of the GS linker tail on each IL-10 monomer increased (Figure 5). We performed our analyses on 11⁺ IL-10 homodimer ions due to their more compact structure compared to higher charge states observed and to avoid overlap with IL-10 monomer ions (Figure S11).

When comparing the CIU fingerprints for two of the linker variants detected, we observe a transitional CIU feature (Figure 5A) that is irreproducible across different fingerprints recorded for linker variants. As such, we have implemented a feature skipping approach to enable the robust and reproducible assessment of CIU_{50} values available in the remainder of the CIU data sets acquired. ⁷⁴ By implementing this procedure, we detect shifts in CIU50-1 values across linker variants, where an increase in linker length produces a stabilization in IL-10 dimers. By plotting CIU₅₀-1 values as a function of average linker mass, which encompasses all Gly and Ser residues on both IL-10 monomers, we are able to discern a strong, positive quadratic relationship ($R^2 = 0.9819$) between CIU₅₀-1 values and linker mass (Figure 5B). This trend is most likely related to cooperative interactions between linkers of increased length in a manner that increases overall dimer stability and induces changes in IL-10 dimer HOS, in addition to the larger number of degrees of freedom available to IL-10 dimers bearing longer remaining linker sequences. To build upon these observations, we executed a series of pairwise RMSD analyses between the CIU fingerprints recorded for each linker variant as a way to quantify global conformational differences in IL-10 dimers as a function of attached linker length (Figures 5C and S13). The RMSD factor differences shown here were calculated by dividing the RMSD values of each replicate by the average RMSD baseline obtained for technical replicates of IL-10 homodimer variants that contained one Ser residue on each monomer. Overall, we obtain a strong positive linear relationship ($R^2 = 0.9923$) when plotting RMSD factor differences as a function of average linker mass. We attribute these observed RMSD factor differences to the same factors as discussed above in our CIU₅₀-1 data. Although these trends in stability represent global shifts in IL-10 dimer HOS and stability as a product of incomplete enzymatic digestion of GS linkers within the intact Fc-IL-10 construct, we are able to reproduce them with other GlySERIAS digests performed using similar reaction con-

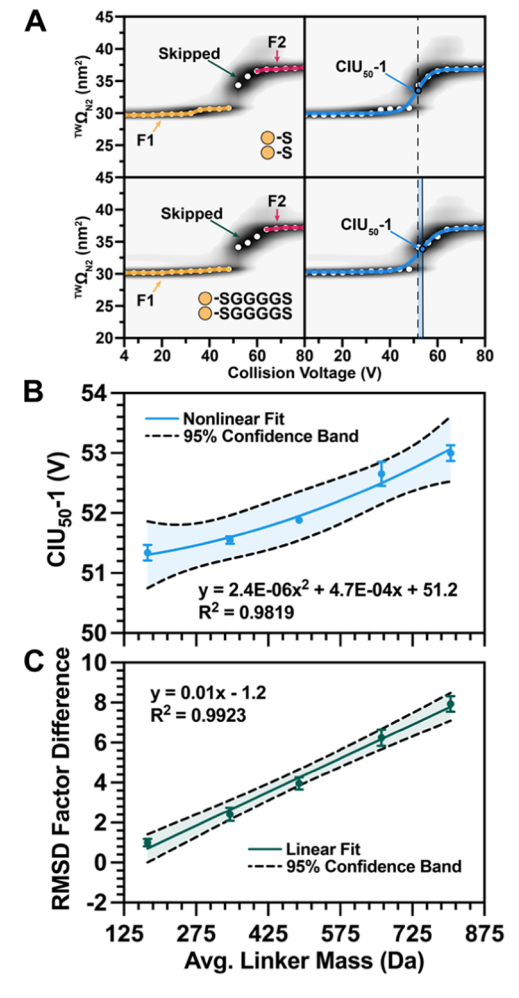


Figure 5. CIU of different Gly-Ser linker variants of IL-10 homodimer. (A) Representative CIU fingerprints of charge state 11^+ demonstrating the transitional state omitted using the feature skipping function deployed within our version of CIUSuite 2 (v2.3). Subsequent CIU $_{50}$ -1 sigmoidal curve fitting reveals subtle shifts in stability between linker variants. (B) Plot of CIU $_{50}$ -1 as a function of average linker mass. Averaged CIU $_{50}$ -1 values (n=3) were fitted with a quadratic function. (C) Plot of RMSD factor difference as a function of average linker mass. Averaged factor differences (n=3) were fitted with a linear function. 95% confidence intervals (dashed lines) are displayed.

ditions (Figure S14). We interpret the small differences in CIU_{50} -1 values recorded between data sets as resulting from different levels of desolvation experienced by ions prior to cIM-MS and CIU analysis. To the best of our knowledge, these studies constitute the first time that the effects of flexible linker lengths on biotherapeutic stability have probed at the level of molecular specificity enabled by MS.

CONCLUSIONS

In this report, we describe a series of IM-MS and CIU measurements that, for the first time, thoroughly probe the HOS and stability of a model Fc-IL-10 fusion protein engineered using flexible Gly-Ser linkers. We find that Fc-IL-10 is substantially more flexible and conformationally dynamic when compared to a series of protein standards and IgG fragments. This high degree of flexibility is partly due to the increased mobility induced by flexible Gly-Ser linkers as well as the conformational polydispersity of IL-10 dimers. The

intricate HOS of Fc-IL-10 is further probed using CIU, where we observe a broad range of features that result from structural changes within Fc and IL-10 subunits upon collisional activation. By using a combination of enzymatic approaches that alter glycosylation patterns and isolate individual Fc and IL-10 domains, we are able to assign lower- and higher-energy CIU transitions of Fc-IL-10 to the unfolding of the IL-10 homodimer and Fc regions of the fusion protein, respectively.

Importantly, we extend the capabilities of IM-MS and CIU to probe the local effects of Gly-Ser linkers on the HOS and stability of IL-10 homodimer, which is the biologically active form of IL-10. Our results reveal a strong positive, quadratic relationship between average linker mass and gas-phase stability, revealing that Gly-Ser linkers cooperatively impact IL-10 homodimer HOS and stability. However, we acknowledge that the CIU₅₀ values shown in Figures 5B and S14A for IL-10 homodimer might have a higher degree of uncertainty than the errors reported. In this case, performing these experiments across different days and capillaries would be beneficial. Taken together, our results further validate the usefulness of IM-MS and CIU in performing fast, informationrich HOS measurements within the biopharmaceutical pipeline. Ongoing efforts in our group are leveraging the multipass and mobility selection functionalities of the cIM platform to gain further insights into the structural polydispersity of Fc-IL-10. Leveraging IM-selected-CIU (IM-CIU), for example, would provide further insights regarding the CIU pathways of different IL-10 homodimer ion precursors. Future efforts in our research group aim to extend these technologies to the characterization of other Fc-fusion protein formats, including those engineered with rigid and cleavable linkers, as well as establish connections between gas-phase and solution-phase unfolding pathways. Finally, we anticipate developing computational approaches to better interpret and predict the CIU pathways of this diverse class of protein therapeutics. Overall, we envision that the workflows demonstrated here will further enable the characterization of novel Fc-fusion proteins and promote the optimization of engineering methods for improved biomolecular stability and efficacy.

ASSOCIATED CONTENT

Supporting Information

The Supporting Information is available free of charge at https://pubs.acs.org/doi/10.1021/acs.analchem.4c01408.

Structure and primary sequence of Fc-IL-10; comparison of experimental and literature $^{\rm TW}\Omega_{\rm N2}$ values; CIU fingerprints of Fc-IL-10 and NISTmAb; native orbitrap spectra of Fc-IL-10 and its subunits; HCD MS/MS spectra of IL-10 homodimer and partially reduced Fc; cIM-MS spectrum of Fc-IL-10 digested with GlySE-RIAS; cyclic $^{\rm TW}\Omega_{\rm N2}$ distributions and stability analysis of Fc and IL-10 homodimer subunits; RMSD plots comparing different linker variants of IL-10 homodimer; plots of CIU $_{50}$ -1 and RMSD factor differences as a function of average linker mass; cIM sequence settings; summary of experimental and literature $^{\rm TW}\Omega_{\rm N2}$ values, as well as deconvoluted masses obtained from Orbitrap MS experiments (PDF)

AUTHOR INFORMATION

Corresponding Author

Brandon T. Ruotolo — Department of Chemistry, University of Michigan, Ann Arbor, Michigan 48109, United States; orcid.org/0000-0002-6084-2328; Phone: 1-734-6150198; Email: bruotolo@umich.edu; Fax: 1-734-615-3718

Authors

- Rosendo C. Villafuerte-Vega Department of Chemistry, University of Michigan, Ann Arbor, Michigan 48109, United States
- Henry W. Li Department of Chemistry, University of Michigan, Ann Arbor, Michigan 48109, United States
- Addison E. Bergman Department of Chemistry, University of Michigan, Ann Arbor, Michigan 48109, United States
- Thomas R. Slaney Analytical Development and Attribute Sciences, Biologics Development, Global Product Development and Supply, Bristol Myers Squibb, New Brunswick, New Jersey 08903, United States; orcid.org/0000-0003-4938-5821
- Naresh Chennamsetty Analytical Development and Attribute Sciences, Biologics Development, Global Product Development and Supply, Bristol Myers Squibb, New Brunswick, New Jersey 08903, United States
- Guodong Chen Analytical Development and Attribute Sciences, Biologics Development, Global Product Development and Supply, Bristol Myers Squibb, New Brunswick, New Jersey 08903, United States
- Li Tao Analytical Development and Attribute Sciences, Biologics Development, Global Product Development and Supply, Bristol Myers Squibb, New Brunswick, New Jersey 08903, United States; © orcid.org/0000-0002-9343-7011

Complete contact information is available at: https://pubs.acs.org/10.1021/acs.analchem.4c01408

Author Contributions

R.V.V., B.T.R., T.R.S., G.C., N.C., and L.T. designed and conceived the experiments described. R.V.V. collected all data and prepared the manuscript. H.W.L. assisted in collecting and analyzing Synapt G2 data. A.E.B. led cIM-MS method development and assisted in cIM-MS and CIU data collection and analysis. T.R.S., N.C., G.G., and L.T. provided the Fcfusion protein characterized in this work. The manuscript was written through contributions of all authors. All authors have given approval to the final version of the manuscript.

Notes

The authors declare no competing financial interest.

ACKNOWLEDGMENTS

This work was supported through findings provided by Bristol Myers Squibb, the UM Biosciences Initiative in support of the UM Biological Mass Spectrometry Facility, and the National Science Foundation (NSF, 2304961), supplied by the Chemical Measurement and Imaging Program in the Division of Chemistry, with partial cofunding from the Division of Molecular and Cellular Biosciences.

REFERENCES

(1) Hoffman, H. M.; Yasothan, U.; Kirkpatrick, P. Nat. Rev. Drug Discovery 2008, 7 (5), 385-386.

- (2) Fenaux, P.; Platzbecker, U.; Mufti, G. J.; Garcia-Manero, G.; Buckstein, R.; Santini, V.; Díez-Campelo, M.; Finelli, C.; Cazzola, M.; Ilhan, O.; et al. *N. Eng. J. Med.* **2020**, 382 (2), 140–151.
- (3) de Oliveira Dias, J. R.; de Andrade, G. C.; Novais, E. A.; Farah, M. E.; Rodrigues, E. B. *Int. J. Retina Vitreous* **2016**, 2 (1), No. 3, DOI: 10.1186/s40942-016-0026-y.
- (4) Czajkowsky, D. M.; Hu, J.; Shao, Z.; Pleass, R. J. EMBO Mol. Med. 2012, 4 (10), 1015–1028.
- (5) Ebrahimi, S. B.; Samanta, D. Nat. Commun. 2023, 14 (1), No. 2411, DOI: 10.1038/s41467-023-38039-x.
- (6) Scheen, A. J. Expert Opin. Biol. Ther. 2017, 17 (4), 485-496.
- (7) Bussel, J. B.; Gerald, S.; Balduzzi, A.; Cooper, N.; Lawrence, T.; Semple, J. W. *Drug Des., Dev. Ther.* **2021**, *15*, 2243–2268.
- (8) de la Croix Ndong, J.; Makowski, A. J.; Uppuganti, S.; Vignaux, G.; Ono, K.; Perrien, D. S.; Joubert, S.; Baglio, S. R.; Granchi, D.; Stevenson, D. A.; et al. *Nat. Med.* **2014**, 20 (8), 904–910.
- (9) Frampton, J. E. Drugs 2021, 81 (17), 2035-2046.
- (10) Goffe, B.; Cather, J. C. J. Am. Acad. Dermatol. 2003, 49 (2), 105-111.
- (11) Wekerle, T.; Grinyó, J. M. Transplant Int. 2012, 25 (2), 139–150.
- (12) Pyzik, M.; Kozicky, L. K.; Gandhi, A. K.; Blumberg, R. S. Nat. Rev. Immunol. 2023, 23 (7), 415–432.
- (13) Rath, T.; Baker, K.; Dumont, J. A.; Peters, R. T.; Jiang, H.; Qiao, S.-W.; Lencer, W. I.; Pierce, G. F.; Blumberg, R. S. Crit. Rev. Biotechnol. 2015, 35 (2), 235–254.
- (14) Zhang, J.; C, J.; Siu, S.; O'Neill, J. W.; Gates, A. H.; Delaney, J.; Mehlin, C. Curr. Pharm. Biotechnol. **2010**, 11 (3), 241–245.
- (15) Carter, P. J. Exp. Cell Res. 2011, 317 (9), 1261-1269.
- (16) Zhang, J.; Yun, J.; Shang, Z.; Zhang, X.; Pan, B. Prog. Nat. Sci. **2009**, 19 (10), 1197–1200.
- (17) Argos, P. J. Mol. Biol. 1990, 211 (4), 943-958.
- (18) Van Rosmalen, M.; Krom, M.; Merkx, M. Biochemistry **2017**, 56 (50), 6565–6574.
- (19) Chen, X.; Zaro, J. L.; Shen, W.-C. Adv. Drug Delivery Rev. 2013, 65 (10), 1357–1369.
- (20) Wriggers, W.; Chakravarty, S.; Jennings, P. A. Peptide Sci. 2005, 80 (6), 736–746.
- (21) Liu, L. J. Pharm. Sci. 2015, 104 (6), 1866-1884.
- (22) Mimura, Y.; Katoh, T.; Saldova, R.; O'Flaherty, R.; Izumi, T.; Mimura-Kimura, Y.; Utsunomiya, T.; Mizukami, Y.; Yamamoto, K.; Matsumoto, T.; Rudd, P. M. *Protein Cell* **2018**, *9* (1), 47–62.
- (23) Wang, W.; Vlasak, J.; Li, Y.; Pristatsky, P.; Fang, Y.; Pittman, T.; Roman, J.; Wang, Y.; Prueksaritanont, T.; Ionescu, R. *Mol. Immunol.* **2011**, 48 (6–7), 860–866.
- (24) Strand, J.; Huang, C. T.; Xu, J. J. Pharm. Sci. 2013, 102 (2), 441–453.
- (25) Castel, J.; Delaux, S.; Hernandez-Alba, O.; Cianferani, S. J. Pharm. Biomed. Anal. 2023, 236, No. 115696.
- (26) Chen, G.; Tao, L.; Li, Z. Drug Discovery Today 2022, 27 (1), 196-206.
- (27) Christofi, E.; Barran, P. Chem. Rev. 2023, 123 (6), 2902-2949.
- (28) Ruotolo, B. T.; Benesch, J. L. P.; Sandercock, A. M.; Hyung, S.-J.; Robinson, C. V. *Nat. Protoc.* **2008**, 3 (7), 1139–1152.
- (29) Dixit, S. M.; Polasky, D. A.; Ruotolo, B. T. Curr. Opin. Chem. Biol. 2018, 42, 93-100.
- (30) Botzanowski, T.; Hernandez-Alba, O.; Malissard, M.; Wagner-Rousset, E.; Deslignière, E.; Colas, O.; Haeuw, J.-F.; Beck, A.; Cianférani, S. *Anal. Chem.* **2020**, *92* (13), 8827–8835.
- (31) Tian, Y.; Han, L.; Buckner, A. C.; Ruotolo, B. T. Anal. Chem. **2015**, 87 (22), 11509–11515.
- (32) Pisupati, K.; Benet, A.; Tian, Y.; Okbazghi, S.; Kang, J.; Ford, M.; Saveliev, S.; Sen, K. I.; Carlson, E.; Tolbert, T. J.; et al. *mAbs* **2017**, 9 (7), 1197–1209.
- (33) Vallejo, D. D.; Kang, J.; Coghlan, J.; Ramirez, C. R.; Polasky, D. A.; Kurulugama, R. T.; Fjeldsted, J. C.; Schwendeman, A. A.; Ruotolo, B. T. *Anal. Chem.* **2021**, 93 (48), 16166–16174.

- (34) Pisupati, K.; Tian, Y.; Okbazghi, S.; Benet, A.; Ackermann, R.; Ford, M.; Saveliev, S.; Hosfield, C. M.; Urh, M.; Carlson, E.; et al. *Anal. Chem.* **2017**, *89* (9), 4838–4846.
- (35) Villafuerte-Vega, R. C.; Li, H. W.; Slaney, T. R.; Chennamsetty, N.; Chen, G.; Tao, L.; Ruotolo, B. T. *Anal. Chem.* **2023**, 95 (17), 6962–6970.
- (36) Deslignière, E.; Ollivier, S.; Ehkirch, A.; Martelet, A.; Ropartz, D.; Lechat, N.; Hernandez-Alba, O.; Menet, J. M.; Clavier, S.; Rogniaux, H.; et al. *Anal. Chem.* **2022**, 94 (22), 7981–7989.
- (37) Deslignière, E.; Ehkirch, A.; Duivelshof, B. L.; Toftevall, H.; Sjögren, J.; Guillarme, D.; D'Atri, V.; Beck, A.; Hernandez-Alba, O.; Cianférani, S. *Pharmaceuticals* **2021**, *14* (6), No. 498, DOI: 10.3390/ph14060498.
- (38) Tian, Y.; Lippens, J. L.; Netirojjanakul, C.; Campuzano, I. D. G.; Ruotolo, B. T. *Protein Sci.* **2019**, 28 (3), 598–608.
- (39) Marty, M. T.; Baldwin, A. J.; Marklund, E. G.; Hochberg, G. K. A.; Benesch, J. L. P.; Robinson, C. V. *Anal. Chem.* **2015**, *87* (8), 4370–4376.
- (40) Kilpatrick, E. L.; Liao, W. L.; Camara, J. E.; Turko, I. V.; Bunk, D. M. Protein Expr. Purif. **2012**, 85 (1), 94–99.
- (41) Hernández, H.; Robinson, C. V. Nat. Protoc. 2007, 2 (3), 715–726.
- (42) Richardson, K.; Langridge, D.; Dixit, S. M.; Ruotolo, B. T. *Anal. Chem.* **2021**, 93 (7), 3542–3550.
- (43) Giles, K.; Ujma, J.; Wildgoose, J.; Pringle, S.; Richardson, K.; Langridge, D.; Green, M. Anal. Chem. 2019, 91 (13), 8564-8573.
- (44) Eldrid, C.; Ujma, J.; Kalfas, S.; Tomczyk, N.; Giles, K.; Morris, M.; Thalassinos, K. Anal. Chem. **2019**, 91 (12), 7554–7561.
- (45) Polasky, D. A.; Dixit, S. M.; Fantin, S. M.; Ruotolo, B. T. *Anal. Chem.* **2019**, *91* (4), 3147–3155.
- (46) Haynes, S. E.; Polasky, D. A.; Dixit, S. M.; Majmudar, J. D.; Neeson, K.; Ruotolo, B. T.; Martin, B. R. *Anal. Chem.* **2017**, *89* (11), 5669–5672.
- (47) Hall, Z.; Politis, A.; Bush, M. F.; Smith, L. J.; Robinson, C. V. J. Am. Chem. Soc. **2012**, 134 (7), 3429–3438.
- (48) Vallejo, D. D.; Polasky, D. A.; Kurulugama, R. T.; Eschweiler, J. D.; Fjeldsted, J. C.; Ruotolo, B. T. *Anal. Chem.* **2019**, *91* (13), 8137–8146.
- (49) Wojdyr, M. J. J. Appl. Crystallogr. 2010, 43 (43), 1126-1128.
- (50) Carlini, V.; Noonan, D. M.; Abdalalem, E.; Goletti, D.; Sansone, C.; Calabrone, L.; Albini, A. Front. Immunol. 2023, 14, No. 1161067, DOI: 10.3389/fimmu.2023.1161067.
- (51) Saraiva, M.; Vieira, P.; O'Garra, A. J. Exp. Med. 2020, 217 (1), No. e20190418.
- (52) Zdanov, A.; Schalk-Hihi, C.; Gustchina, A.; Tsang, M.; Weatherbee, J.; Wlodawer, A. Structure 1995, 3 (6), 591–601.
- (53) Walter, M. R.; Nagabhushan, T. L. Biochemistry 1995, 34 (38), 12118–12125.
- (54) Josephson, K.; Logsdon, N. J.; Walter, M. R. Immunity 2001, 15 (1), 35–46.
- (55) Minshawi, F.; Lanvermann, S.; McKenzie, E.; Jeffery, R.; Couper, K.; Papoutsopoulou, S.; Roers, A.; Muller, W. Front. Immunol. 2020, 11, No. 1794, DOI: 10.3389/fimmu.2020.01794.
- (56) Syto, R.; Murgolo, N. J.; Braswell, E. H.; Mui, P.; Huang, E.; Windsor, W. T. *Biochemistry* **1998**, *37* (48), 16943–16951.
- (57) Aliyari, E.; Konermann, L. Anal. Chem. 2021, 93 (37), 12748-12757.
- (58) Konermann, L.; Ahadi, E.; Rodriguez, A. D.; Vahidi, S. *Anal. Chem.* **2013**, 85 (1), 2–9.
- (59) Vallejo, D. D.; Jeon, C. K.; Parson, K. F.; Herderschee, H. R.; Eschweiler, J. D.; Filoti, D. I.; Ruotolo, B. T. *Anal. Chem.* **2022**, *94* (18), 6745–6753.
- (60) Campuzano, I. D. G.; Larriba, C.; Bagal, D.; Schnier, P. D.Ion Mobility and Mass Spectrometry Measurements of the Humanized IgGk NIST Monoclonal Antibody. In State-of-the-Art and Emerging Technologies for Therapeutic Monoclonal Antibody Characterization Volume 3. Defining the Next Generation of Analytical and Biophysical Techniques, ACS Symposium Series; ACS Publication, 2015; Vol. 1202, pp 75–112.

- (61) Pacholarz, K. J.; Porrini, M.; Garlish, R. A.; Burnley, R. J.; Taylor, R. J.; Henry, A. J.; Barran, P. E. *Angew. Chem., Int. Ed.* **2014**, 53 (30), 7765–7769.
- (62) Zheng, X.; Kurulugama, R. T.; Laganowsky, A.; Russell, D. H. Anal. Chem. 2020, 92 (10), 7218–7225.
- (63) Niu, S.; Ruotolo, B. T. Protein Sci. 2015, 24 (8), 1272-1281.
- (64) Watanabe, Y.; Vasiljevic, S.; Allen, J. D.; Seabright, G. E.; Duyvesteyn, H. M. E.; Doores, K. J.; Crispin, M.; Struwe, W. B. *Anal. Chem.* **2018**, *90* (12), 7325–7331.
- (65) van Schaick, G.; Dominguez-Vega, E.; Castel, J.; Wuhrer, M.; Hernandez-Alba, O.; Cianferani, S. *Anal. Chem.* **2023**, 95 (8), 3932–3939.
- (66) Zhong, Y.; Han, L.; Ruotolo, B. T. Angew. Chem. **2014**, 126 (35), 9363–9366.
- (67) Eschweiler, J. D.; Martini, R. M.; Ruotolo, B. T. J. Am. Chem. Soc. 2017, 139 (1), 534–540.
- (68) Tian, Y.; Ruotolo, B. T. Int. J. Mass Spectrom. 2018, 425, 1–9, DOI: 10.1016/j.ijms.2017.12.005.
- (69) Upton, R.; Migas, L. G.; Pacholarz, K. J.; Beniston, R. G.; Estdale, S.; Firth, D.; Barran, P. E. *Chem. Sci.* **2019**, *10* (9), 2811–2820.
- (70) Zheng, K.; Bantog, C.; Bayer, R. mAbs 2011, 3 (6), 568-576.
- (71) Hristodorov, D.; Fischer, R.; Joerissen, H.; Müller-Tiemann, B.; Apeler, H.; Linden, L. Mol. Biotechnol. 2013, 53 (3), 326–335.
- (72) Reusch, D.; Tejada, M. L. Glycobiology **2015**, 25 (12), 1325–1334
- (73) Shelimov, K. B.; Clemmer, D. E.; Hudgins, R. R.; Jarrold, M. F. J. Am. Chem. Soc. 1997, 119, 2240–2248.
- (74) Anders, A.; Tidwell, E.; Gadkari, V.; Koutmos, M.; Ruotolo, B. *J. Am. Chem. Soc.* **2024**, *146*, 4412–4420, DOI: 10.1021/jacs.3c09230.